International Symposium
On Turbulence and Shear Flow
Phenomena (TSFP-8)
August 28 - 30, 2013 Poitiers, France

LARGE EDDY SIMULATION OF THE TRANSITION PROCESS FROM REGULAR TO IRREGULAR SHOCK-WAVE/BOUNDARY-LAYER INTERACTION

Jan Matheis, Bernd Budich, Stefan Hickel
Institute of Aerodynamics and Fluid Mechanics
Technische Universität München
jan.matheis@tum.de

ABSTRACT

The transition process from regular to irregular shock-wave/boundary-layer interaction (SWBLI) at $M_\infty = 2$ is studied both numerically and theoretically. The classical two- and three-shock theory is applied for carefully analyzing a data base of well resolved large-eddy simulations (LES). Inviscid theory appears to be a descriptive tool for the interpretation of the highly transient flow field of the SWBLI. Disturbances related to the incoming turbulent boundary layer can be identified as a source of bidirectional transition processes between regular and irregular SWBLI at a critical deflection angle across the incident shock wave.

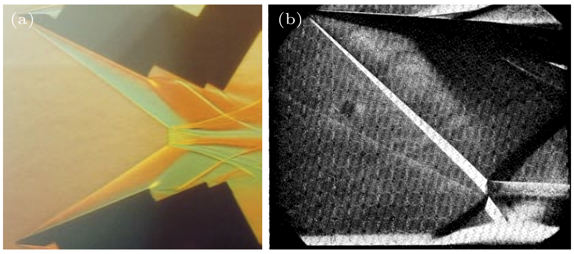

Figure 1: (a) Experimental schlieren image of the quasi-inviscid MR at $M_\infty = 4.96$, $\vartheta_{01} = 28^\circ$ and $\vartheta_{02} = 24^\circ$, courtesy of Li *et al.* (1999). (b) Experimental schlieren image of the ISWBLI at $M_\infty = 1.965$ and $\vartheta_{01} = 15.2^\circ$, courtesy of Bardsley & Mair (1950).

INTRODUCTION

A shock wave represents a highly nonlinear phenomenon. The state of the medium that passes the wave changes instantaneously and irreversibly. The complexity of this process increases when more than one shock occurs, for example, in the case of the interaction of a shock with a symmetry plane, a solid surface or the asymmetric intersection of shock waves. The reflection phenomenon was first described by Ernst Mach in 1887, who experimentally observed two different wave configurations, namely the regular reflection (RR) and the irregular reflection / Mach reflection (MR). The symmetric reflection of shock waves in an inviscid framework can be briefly summarized as follows: Characteristic wave pattern of shock reflections (RR and MR) are restricted to certain domains depending on the free stream Mach number M_∞ and the deflection angle ϑ_{01} across the incident shock. Criteria beyond which RR and MR are theoretically impossible are given by the detachment and the von Neumann condition, respectively; see Ben-Dor (2010) for a comprehensive review. Both RR and MR wave configurations are possible within the parameter space spanned by these two conditions. The existence of such a domain led Hornung *et al.* (1979) to hypothesize that a hysteresis process could exist in the transition process between both wave patterns. As the deflection across the incident shock increases, transition from RR to MR occurs near the detachment criterion, while in the opposite case transition from MR to RR occurs at the von Neumann condition. Recently, asymmetric intersections of shock waves got into the focus of classical gas-dynamic research, such as shown in Fig. 1a, see Li *et al.* (1999) and Hu *et al.* (2009), e.g.. Li *et al.* (1999) proposed transition criteria for the reflection of asymmetric shock waves corresponding to the detachment and von Neumann criteria. In the following, it will become apparent that methods (e.g. shock polars) and transition criteria (ϑ_N, ϑ_D) developed for inviscid flow in the recent decades also constitute a descriptive tool for analyzing the interaction of shock waves with viscous boundary layers.

Shock-wave/boundary-layer interaction (SWBLI) is one of the most prevalent phenomena occurring in high-speed flight and has received much attention in the past decades; see the comprehensive review paper of Delery & Marvin (1986). Geometric configurations are wide-ranging in nature, however, four basic SWBLI configurations can be identified: the ramp flow, the oblique shock reflection, and the forward and backward facing step. Fig. 2a schematically depicts the strong regular SWBLI (RSWBLI) for the case of an oblique shock reflection. The strong interaction is characterized by a noticeable separation of the boundary-layer leading to a wall pressure distribution that clearly exhibits three inflection points. As can be seen in Fig. 2a, the boundary-layer separates well upstream from the point x_{imp} where the incident shock C_1 would impinge in an inviscid flow. The adverse pressure gradient affects the upstream flow through the subsonic layer, causing a displacement of the streamlines away from the wall and eventually boundary layer separation. Compression waves are formed that propagate into the potential outer flow. These compression waves coalesce into the separation shock C_2. It is important to note that the interaction between shock and boundary layer can feature several other phenomena. For a more detailed discussion, see Henderson (1967) and Delery & Marvin (1986), who gave a review of the various types of shock reflections in the presence of a boundary-layer.

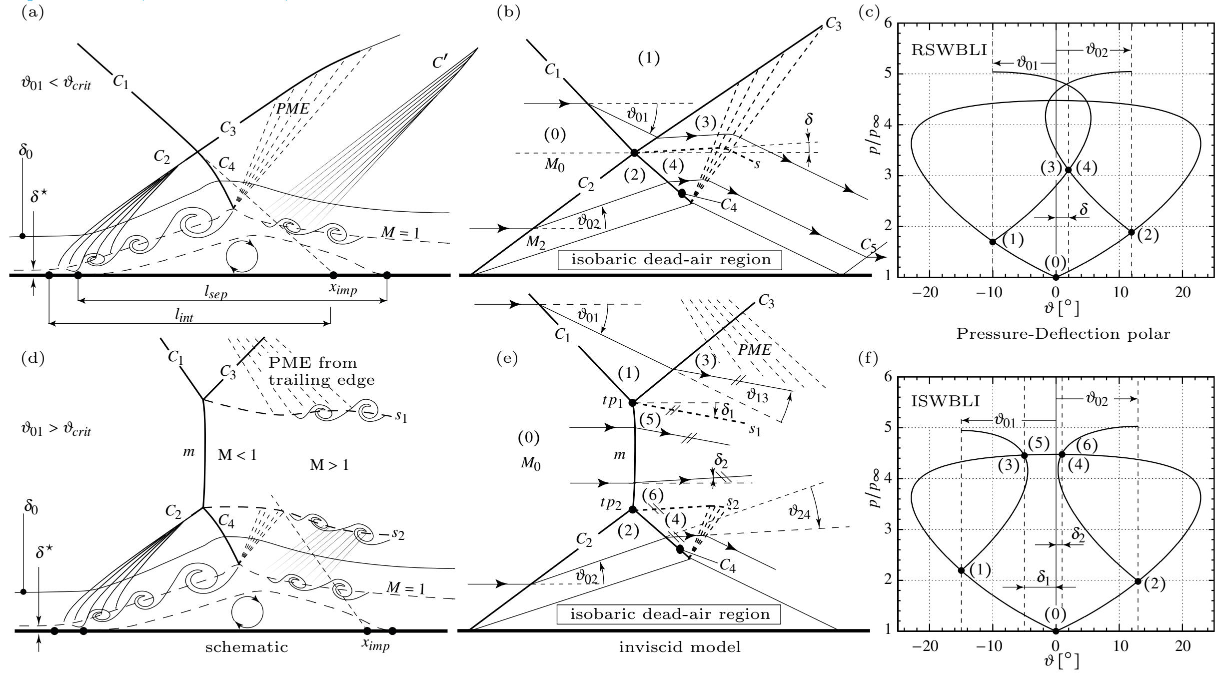

Figure 2: (a) Schematic illustration of the RSWBLI. (b) Inviscid flow model of the RSWBLI with separation, from Delery & Marvin (1986). (c) Shock polar representation of the inviscid flow model for the RSWBLI. (d) Schematic illustration of the *strong* ISWBLI. (e) Inviscid flow model of the ISWBLI with separation. (f) Shock polar representation of the inviscid flow model for the ISWBLI.

Even though viscous effects play a crucial role for SWBLI phenomena, inviscid methods are capable of capturing and describing some of the main physics involved. Fig. 2b shows the inviscid model of the strong RSWBLI adopted from Delery & Marvin (1986). Fig. 2c shows the shock polar representation of this model. If the deflection across C_1 and C_2 is known, the shock polar analysis allows for a precise prediction of the states downstream of the reflected shocks C_3 and C_4. However, while the deflection across C_1 is generally defined by a boundary condition, the deflection across C_2 is a priori unknown. Analogously, Fig. 2d-f illustrates the irregular SWBLI (ISWBLI) as a schematic, an inviscid model and in the shock polar representation. When the deflection across C_1 exceeds a critical value ϑ_{crit}, the regular intersection of C_1 and C_2 becomes impossible. As a consequence, a Mach stem m is formed, connecting the lambda food C_2/C_4 and the shocks C_1/C_3. Again, the states downstream of the two triple-points tp_1 and tp_2 can be determined by shock polars (Fig. 2f). As indicated in Fig. 2e, the deflection across C_1 and C_2 may not necessarily be symmetric. Therefore, the theory on the intersection of asymmetric shocks is important for understanding SWBLI.

The aforementioned phenomena have been investigated in great depth, however, it is worth mentioning that the Mach reflection, and the investigation of transition criteria in particular, were treated mostly in an inviscid framework. It is argued that setups leading to inviscid interactions resemble the inlet geometry of supersonic vehicles (see e.g. Li & Ben-Dor, 1997) . Indeed, inlet geometries, which can be treated as inviscid, may exist, however, in many aeronautical applications a symmetric inlet design is not intended. If one considers typical Scramjet designs (X51-A, HyShot), it becomes apparent that any assumption involving only the symmetric/asymmetric intersection of shocks is far off reality. On the other hand, the SWBLI was mainly studied at sufficiently small deflection angles, where transition processes to ISWBLI can be disregarded. For double-wedge configurations, it is well known that the Mach stem can move upstream and ultimately out of the inlet if the geometry itself does not support a stable Mach reflection (see e.g. Li & Ben-Dor, 1997). It is expected that the same process can occur in ISWBLI and is therefore crucial with regard to the unstart of supersonic inlets and Scramjet engines at off-design conditions.

Table 1: Summary of relevant parameters.

	$SWBLI_1$	$SWBLI_2$	$SWBLI_3$	$SWBLI_4$	$SWBLI_5$
ϑ_{01} [°]	11.0	12.0	12.5	13	14
β_{01} [°]	40.423	41.575	42.169	42.775	44.029
x_{exp}	−4.199	−3.307	−2.855	−2.397	−1.462
$FTT_t{}^a$	37.63	30.41	24.91	30.39	37.04
$FTT_s{}^b$	29.63	16.68	11.38	15.05	24.37
$N_t{}^c$	1681	2433	1993	2430	2963
$N_s{}^d$	23707	13346	9104	12067	19496
$\langle\beta_{02}\rangle^e$	40.0	41.0	41.0	41.0	41.1
$\langle\vartheta_{02}\rangle^f$	10.53	11.41	11.41	11.41	11.50
l_0	8.44	10.55	11.69	12.55	14.83
l_{sep}	9.77	11.64	13.39	14.20	16.61

[a] Total simulation time in flow through times (FTT). [b] FTT's used for the time averaged flow field with an internal sample interval of 0.05 δ_{ref}/u_∞. [c] Total number of instantaneous snapshots gathered with a sample interval of 0.5 δ_{ref}/u_∞. [d] Total number of samples used for the time averaged flow field. [e] Shock angle $\langle\beta_{02}\rangle$ measured from the time averaged flow field with respect to $\langle\vartheta_0\rangle = 0.2$. [f] Deflection across separation shock calculated from $\langle\beta_{02}\rangle$ with $\langle M_\infty\rangle = 1.995$.

To our knowledge, ISWBLI has been observed only in experiments, see Fig. 1b, but not yet studied numerically. Furthermore, it appears that very little information is available regarding the transition process in viscous flows. Since classical inviscid gas dynamics and SWBLI share a common ground, the intention of this study is to make use of both methods in order to describe the transition from RSWBLI to ISWBLI.

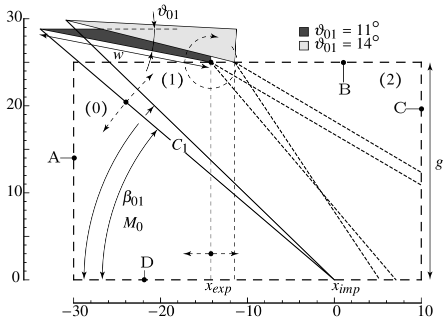

Figure 3: Schematic of the numerical setup.

SETUP

Numerical Model

We performed implicit large-eddy simulations (ILES) that resolve the transition process from RSWBLI to ISWBLI in time and space. The compressible Navier-Stokes equations are discretized by a conservative finite-volume method using the compressible adaptive local deconvolution method (ALDM) for the convective fluxes, which also acts as a subgrid-scale turbulence model (Hickel & Larsson, 2009), while the diffusive fluxes are computed using a 2$^{\text{nd}}$-order central differencing. For the fluid, an ideal gas assumption in conjunction with Sutherlands law for temperature-viscosity dependence is utilized.

Geometry and Numerical Setup

Fig. 3 illustrates the investigated geometry and the numerical domain. We consider a supersonic TBL characterized by a free-stream Mach number of $M_\infty = 2.0$ and a Reynolds number based on the boundary layer thickness at the theoretical inviscid impingement point x_{imp} of $Re_{\delta_{imp}} \approx 48.3 \cdot 10^3$. The present study focuses on the oblique shock reflection, which is realized by a wedge inclined at an angle ϑ_{01} relative to the incoming flow. All computations have been performed in a rectangular domain, which extends for $L_x = 40\delta_{ref}$, $L_y = 25\delta_{ref}$, $L_z = 4\delta_{ref}$ in the streamwise, wall-normal and spanwise directions with δ_{ref} being the boundary layer thickness for which $Re_{\delta_{ref}} = \rho_\infty u_\infty \delta_{ref}/\mu_\infty = 33.7 \cdot 10^3$. The computational domain is discretized with $N_x = 520$, $N_y = 600$, $N_z = 100$ cells, thus leading to a total number of $31.2 \cdot 10^6$ elements. In wall-normal direction, a tanh line bunching law is used with a stretching factor of $\beta_y = 2.55$. The discretization yields resolutions of $\Delta x^+ \approx 38$, $\Delta y^+_{min} \approx 1.3$ and $\Delta z^+ \approx 20$. At the inlet (A) the digital-filter technique (Klein & Sadiki, 2003) is employed for prescribing turbulent inflow data. At the surface (B) an inflow boundary condition based on Riemann invariants is imposed, with the prescribed aerodynamic and thermodynamic state upstream (0) and downstream (1) of C_1 and downstream of the centered Prandtl-Meyer expansion (PME) emanating from the trailing edge of the wedge (2). At the outlet (C), a linear extrapolation procedure of all flow variables is used. The wall (D) is isothermal at the nominal adiabatic temperature $T_w/T_\infty = 1.8$ with a recovery factor of $r = 1$.

Altogether, five ILES have been performed, with an deflection angle $\vartheta_{01} = [11°, 12°, 12.5°, 13°, 14°]$ (hereafter referred to as $SWBLI_{1/2/3/4/5}$). Three features concerning the shock generator geometry definition have been deemed relevant. First, it is important to ensure that proper scaling can be applied to characteristic length scales of the SWBLI (e.g. separation length l_{sep}). By keeping the inviscid impingement location constant, TBL characteristics at x_{imp}, e.g. $\delta_{0,imp}$, offer a reasonable characteristic length scale. Second, the wedge width w is to be kept constant in order to describe a realistic experimentally reproducible geometry. To meet both requirements, the shock generator is simultaneously shifted horizontally and rotated around its trailing edge as ϑ_{01} increases. The last important feature concerns the PME. The ratio of channel height to wedge width $g^+ = g/w$ determines at which x-coordinate, with respect to x_{imp}, the first characteristic of the PME impinges on the flat plate. In the present study, this position was considered to be of great importance for mainly two reasons. The PME has a major effect on the spatial extent of the separated region, because it significantly reduces the adverse pressure gradient felt by the TBL. The second reason concerns the simulations in which an ISWBLI is obtained. In an inviscid framework, it is well known that the Mach stem height (MSH) normalized by the wedge width w can be expressed as $m^+ = f^+(M_\infty, \gamma, g^+, \vartheta_{01})$, where f^+ is an unknown non-dimensional function (see e.g. Hornung, 1982; Li & Ben-Dor, 1997). In other words, the MSH is associated with the characteristic length scale g^+. In the present study the TBL itself provides an additional characteristic length scale. Up to the present date, it remains open to what extend the MSH is influenced by TBL characteristics (e.g. Re_{δ_i}, c_f...),which are inherently connected with the length scales resulting from the SWBLI itself (e.g. l_{sep}). In an inviscid framework, it can be shown that m^+ decreases as g^+ increases (see e.g. Li & Ben-Dor, 1997) , provided all other variables are held constant. Since the flow topology must fit well within the computational domain, g^+ was set to $5/4$ in all simulations, which results in a relatively small Mach stem. In summary, the boundary conditions for each simulation are fully determined by prescribing the deflection ϑ_{01}, the wedge width w, channel height g, and the axial position of the trailing edge x_{exp} with respect to the nominal inviscid impingement point x_{imp}. All relevant geometric parameters are listed in Table 1.

RESULTS AND DISCUSSION

Statistical properties have been obtained by averaging in time and spanwise direction with equally spaced time samples of the flow field at time intervals $0.05\delta_{ref}/u_\infty$ after an initial transient. To enable transient post-processing, three-dimensional snapshots have been gathered with a sample interval of $0.5\delta_{ref}/u_\infty$. A general overview of two characteristic length scales is given in Fig. 4. The time-averaged skin friction and wall pressure distributions evidently show that separation length l_{sep} and interaction length l_0 increase as the shock strength increases. The cases $SWBLI_{3/4/5}$ exhibit a constant pressure plateau, whereas the cases $SWBLI_{1/2}$ only show an inflection point in the wall pressure distribution. Note that the maximum wall pressure is significantly smaller than it would be across an inviscid reflection (without any PME downstream) due to the pressure drop caused by the expansion emanating from the trailing edge of the wedge. The theoretical inviscid impingement point of the leading characteristic of the PME is indicated by a square (▫) in Fig. 4b. The PME has a major effect on the obtained interaction length l_0 and thereby enables the simulation of SWBLI at such strong shock strengths.

$SWBLI_{1/5}$ were simulated independently of each other to determine the boundaries in which the transition process

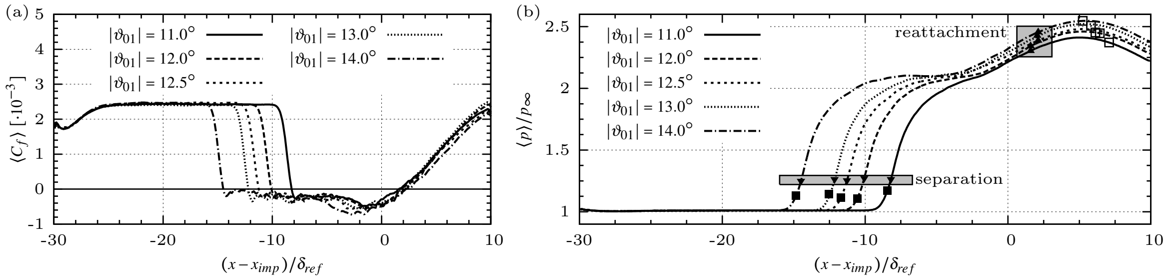

Figure 4: (a) Time-averaged skin friction distribution for the cases $SWBLI_{1/2/3/4/5}$. (b) Time-averaged wall pressure signal for the cases $SWBLI_{1/2/3/4/5}$. ▾ onset of separation. ▴ reattachment of the separated flow. ▪ $x-$coordinate defining the interaction length. ▫ $x-$coordinate at which the first characteristic of the PME impinges on the wall.

takes place. From those simulations, it was found that transition is expected to occur between a deflection of 12° and 13° across the incident shock C_1. Then, the simulations $SWBLI_{2,3,4}$ were set up to more precisely determine the point of transition. To exclude a transition process initiated by initial conditions, simulation $SWBLI_i$ was initialized with a quasi-steady flow field obtained from simulation $SWBLI_{i-1}$. Fig. 5 shows the mass fluid per unit span within the separation zone to illustrate simulation time, initial transients and number of samples gathered for the cases $SWBLI_{2,3,4}$. 30.41, 24.91 and 30.39 flow through times (FTT) has been simulated for the cases $SWBLI_{2,3,4}$, respectively. Fig. 7 gives an impression of the time-averaged flow field of the interaction by means of contour plots of the density gradient magnitude for the cases $SWBLI_{1/2/3/5}$. Isocontour levels of constant local flow direction are plotted with respect to the undisturbed potential flow upstream of the incident shock. Two alternatives to determine the deflection $\langle\vartheta_{02}\rangle$ across the separation shock C_2 exist: (a) based on the measured shock angle $\langle\beta_{02}\rangle$ and (b) based on the isocontour levels of constant local flow direction. Method (a) has proven to be more reliable, whereas method (b) strongly depends on the visualization method to extract the shock 'thickness'. Table 1 summarizes the obtained values for the separation shock angle $\langle\beta_{02}\rangle$, measured with respect to a mean deflection $\langle\vartheta_0\rangle = 0.2°$ upstream of C_2 (due to the displacement effect of the TBL upstream of the interaction). Based on $\langle\beta_{02}\rangle$ and a pre-shock Mach number $\langle M_0\rangle = 1.995$, we can calculate the deflection across C_2 with the help of the oblique shock relations. It is noteable that, within the limits of accuracy of the measurements, the time-averaged shock angle $\langle\beta_{02}\rangle$ and, hence, deflection across the separation shock $\langle\vartheta_{02}\rangle$ remain constant for the cases $SWBLI_{2/3/4/5}$. A similar observation was made by Green (1970), who stated that once separation has occured, the shock strength of the separation shock C_2 is independent of the incident shock that causes separation. Similar characteristics were also found for the ramp flow which bears a certain resemblance to the oblique shock reflection (see Delery & Marvin, 1986). As a consequence, transition to ISWBLI in a 'time-averaged' context has to be expected at deflection angles greater than $\langle\vartheta_{01}\rangle \approx 14°$ across the incident shock (for $\langle\vartheta_{02}\rangle = 11.41°$ the corresponding detachment criterion for asymmetric shock wave intersections is given by $\langle\vartheta_D\rangle = 14.21°$). The present study however reveals that this is not the case. Transition to ISWBLI occurred unambiguously at a nominal deflection across C_1 equal to 13° ($SWBLI_4$). Even at 12.5° ($SWBLI_3$), the flow partially exhibits characteristics of the ISWBLI. A closer look to transient data reveals that fluctuations related to the incoming TBL trigger transition from RSWBLI to ISWBLI. Fig. 8a-c show the transient signal of the spanwise averaged flow direction upstream of the intersection ϑ_0, the absolute deflection $|\vartheta_{01}|$ across the incident shock C_1 and the deflection ϑ_{02} across the separation shock C_2 (with respect to $\langle\vartheta_0\rangle = 0.2$) for the cases $SWBLI_{3/4}$. The signal was recorded by placing probes relative to the intersection point of C_1 and C_2. For this purpose a postprocessing-algorithm was developed that tracks the points of shock intersection in time and space. The positions of the probes at time instance $t_1 = 2257$ are indicated in Fig. 8d. From the recorded signal (Fig. 8c), the mean deflection across C_2 for the cases $SWBLI_{3/4}$ is found to be $\langle\vartheta_{02}^{12.5°}\rangle = 11.96°$ and $\langle\vartheta_{02}^{13.0°}\rangle = 11.84°$. This value is in good agreement with the values obtained by relying on the time-averaged shock angle $\langle\beta_{02}\rangle$. This result indicates that the deflection across C_2 is almost precisely represented by the recorded signal. Furthermore, the fact that $\langle\vartheta_{02}^{12.5°}\rangle \approx \langle\vartheta_{02}^{13.0°}\rangle$ confirms the observation that the shock strength of the separation shock C_2 is independent of the incident shock C_1. Applying classical inviscid theory on the results, the intersection between C_1 and C_2 is supposed to be regular. However, as already mentioned, transition to ISWBLI occurred unambiguously at a nominal deflection of $\vartheta_{01} = 13°$ across C_1. Fig. 8d illustrates the instantaneous flow field at $t_1 = 2257$. A clear Mach stem and two shear layers emanating from the triple points can be identified, therefore, transition has occurred for $t < t_1$. Fig. 8e shows the flow field at $t_2 = 2341$. Since two shear layers are still visible this situation also constitutes a ISWBLI, however, the Mach stem appears to be in-

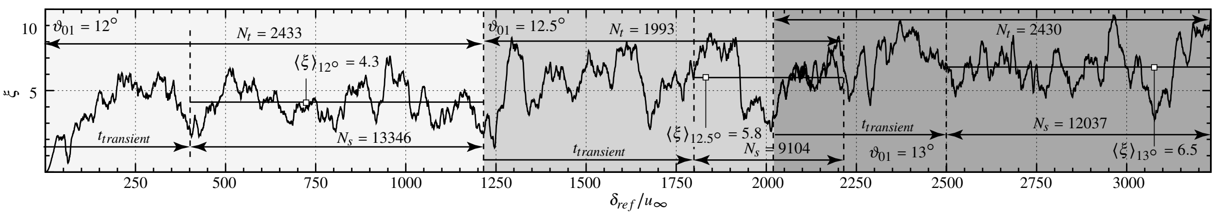

Figure 5: Evolution of the fluid mass per unit span within the separation zone for the cases $SWBLI_{2/3/4}$.

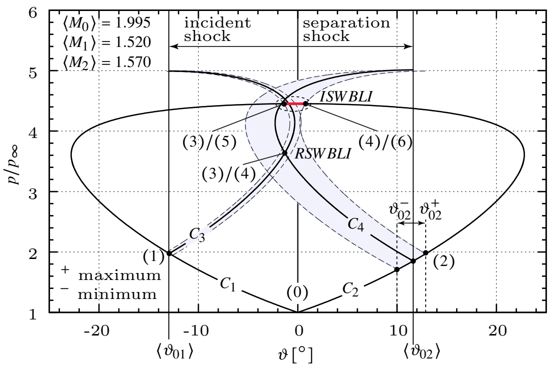

Figure 6: Shock polar representation of the intersection of incident shock C_1 and separation shock C_2 for case SWBLI$_4$. Numbering of the states according to Fig. 2.

finitesimal small. This observation can be explained as follows: First, the deflection across C_2 appears to be highly transient, with significant deviations from its mean value ($\vartheta_{02,max}^{13.0°} = 12.88$, $\vartheta_{02,min}^{13.0°} = 10.08$). A similar transient character is observed for the recorded signals upstream of the intersection (ϑ_0) and downstream of the incident shock C_1 ($|\vartheta_{01}|$), see Fig. 8a-b. As a consequence, the intersection of C_1 and C_2 can become both possible and impossible, see Fig. 6, within an transient inviscid framework. Second, it is well known that the low-frequency unsteadiness of the separated region leads to a shift of the separation shock C_2 up- and downstream of its mean position. For these reasons, and based on geometric considerations, the MSH can not remain constant in the context of SWBLI. Such events, namely the growth/shrinking of the Mach stem for case SWBLI$_4$ or the appearance of two slip lines with an infinitesimal small Mach stem for case SWBLI$_3$, can be observed at several points in time.

The interaction between incident shock C_1 and separation shock C_2 is illustrated by means of shock polars for case SWBLI$_4$ in Fig. 6. The free-stream polar is plotted for a mean Mach number $\langle M_0 \rangle = 1.995$ (compression waves emanating from the TBL slightly decrease the free stream Mach number) upstream of the interaction. The numbering of the states (1) – (6) is according to Fig. 2. In addition, two grey shaded regions enclosed by dashed dotted lines denote the variation of deflection angles that were observed across C_1 and C_2. Obviously, the mean-interaction does constitute a RSWBLI (the polars C_3 and C_4 have an intersection point at (3)/(4)). However, only an ISWBLI is possible in the area indicated by the red line connecting (3)/(5) and (4)/(6). Therefore, the growth and shrinking of the Mach stem can clearly be assigned to fluctuations related to the incoming TBL.

Fig. 9 shows the temporal evolution of the fluid mass per unit span ξ enclosed within the separation zone and the variation of the MSH h_M for case SWBLI$_5$. As already explained, the MSH does not remain constant and deviations of up to 20% from its mean value are observed. The separation shock C_2 is moving up- and downstream due to a low-frequency unsteadiness of the separated region. Grilli *et al.* (2011) argued that this movement is driven by periodic increase and decrease of the enclosed fluid mass. From a geometrical point of view such a process can also explain a decreasing/increasing Mach stem. A coupling of the mass fluid within the separation zone and MSH can clearly be identified in Fig. 9. However, the whole mechanism is not entirely understood at this time. In particular, the MSH is expected to be influenced also by the instantaneous shock angles β_{01} and β_{02}.

CONCLUSIONS

The transition process from regular to irregular SWBLI was studied. It was shown that for the considered flow conditions ($M_\infty = 2$ and $\mathrm{Re}_{\delta_{imp}} \approx 48.3 \cdot 10^3$) transition occurs at a nominal deflection of 13° across the incident shock. The time-averaged shock strength of the separation shock appears to be decoupled from the incident shock, which is in agreement with the observations made in earlier experiments (Green, 1970). However, the observation of an irregular SWBLI at a nominal deflection of 12.5° indicates that turbulent fluctuations trigger transition. We further corroborated this interpretation through a shock polar analysis that takes into account perturbations related to the incoming TBL. It was shown that the Mach stem height does not remain constant. Fluctuations of the height are coupled to the dynamics of the shock induced boundary layer separation.

REFERENCES

Bardsley, O. & Mair, W.A. 1950 III. The interaction between an oblique shock-wave and a turbulent boundary-layer. *Philosophical Magazine Series 7* **42** (324), 29–36.

Ben-Dor, G. 2010 *Shock Wave Reflection Phenomena*. Springer Verlag.

Delery, J. & Marvin, J. G. 1986 Shock-wave boundary layer interactions. AGARD-AG-280. *Tech. Rep.*.

Green, J. E. 1970 Reflexion of an oblique shock wave by a turbulent boundary layer. *Journal of Fluid Mechanics* **40** (Part 1), 81–95.

Grilli, M., Schmid, P. J., Hickel, S. & Adams, N. A. 2011 Analysis of unsteady behaviour in shockwave turbulent boundary layer interaction. In *Proceedings of the 7th European Symposium on Aerothermodynamics*, pp. 1–7.

Henderson, L. F. 1967 The reflexion of a shock wave at a rigid wall in the presence of a boundary layer. *Journal of Fluid Mechanics* **30** (04), 699–722.

Hickel, S. & Larsson, J. 2009 On implicit turbulence modeling for LES of compressible flows. In *Advances in Turbulence XII* (ed. Bruno Eckhardt), *Springer Proceedings in Physics*, vol. 132, pp. 873–875. Springer.

Hornung, H. G. 1982 Transition from regular to Mach reflection of shock waves Part 2. The steady-flow criterion. *Journal of Fluid Mechanics* **123**, 155–164.

Hornung, H. G., Oertel, H. & Sandeman, R. J. 1979 Transition to Mach reflexion of shock waves in steady and pseudosteady flow with and without relaxation. *Journal of Fluid Mechanics* **90** (3), 541–560.

Hu, Z. M., Myong, R. S. & Kim, MS 2009 Downstream flow condition effects on the RR - MR transition of asymmetric shock waves in steady flows. *Journal of Fluid Mechanics* **620**, 43–62.

Klein, M. & Sadiki, A. 2003 A digital filter based generation of inflow data for spatially developing direct numerical or large eddy simulations. *Journal of Computational Physics* .

Li, H. & Ben-Dor, G. 1997 A Parametric Study of Mach Reflection in Steady Flows. *Journal of Fluid Mechanics* **341**, 101–125.

Li, H., Chpoun, A. & Ben-Dor, G. 1999 Analytical and experimental investigations of the reflection of asymmetric shock waves in steady flows. *Journal of Fluid Mechanics* **390**, 43.

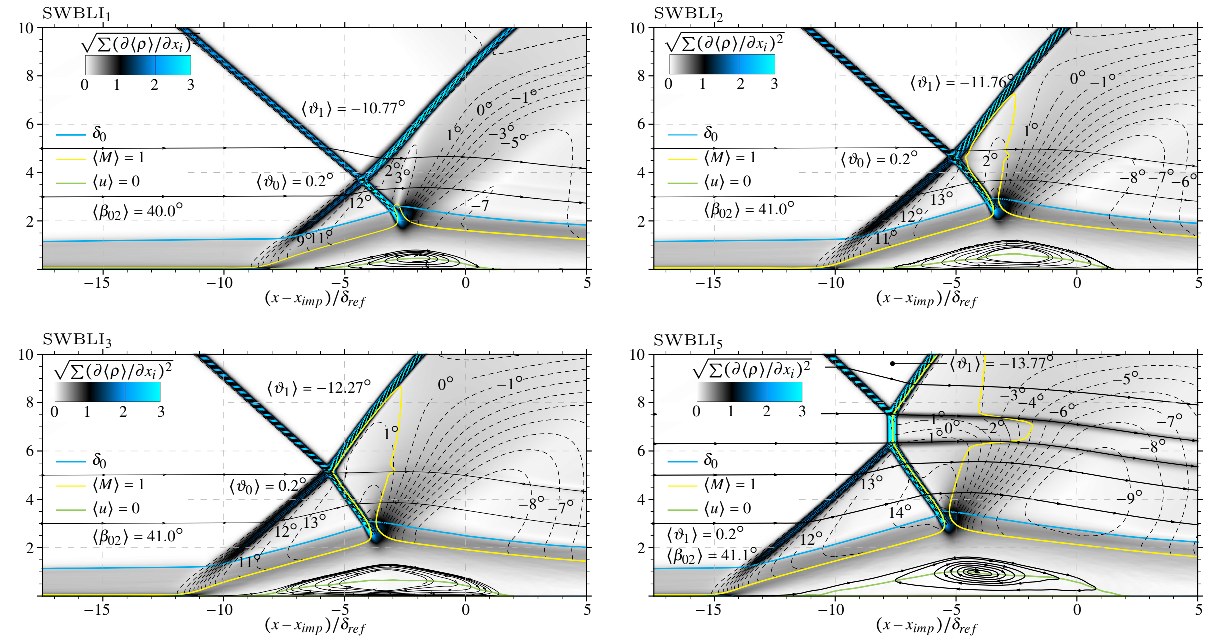

Figure 7: Illustration of the interaction zone for the cases $\mathrm{SWBLI}_{1/2/3/5}$ by means of a contour plot of the time- and spanwise-averaged density gradient magnitude. Isocontour levels of constant local flow direction are plotted and labeled with the corresponding angle with respect to the undisturbed potential flow upstream of the incident shock C_1. Boundary layer edge, subsonic region and region of reverse flow are indicated by the cyan blue, yellow and green line, respectively.

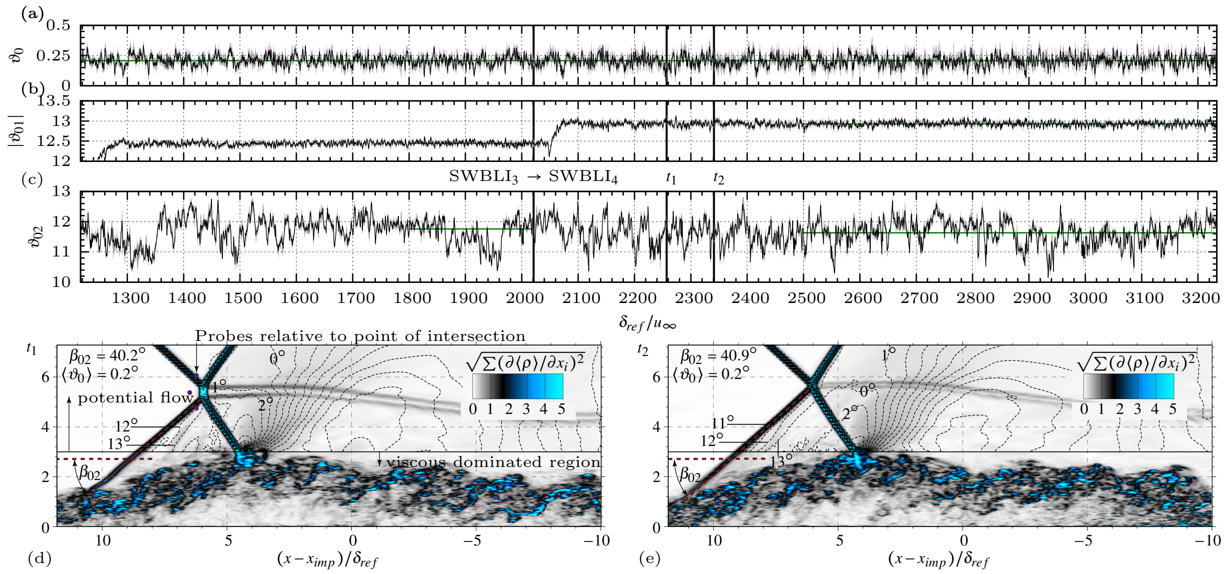

Figure 8: $(a)-(c)$: —— Transient signal of the spanwise averaged flow direction upstream of the interaction ϑ_0, the deflection $|\vartheta_{01}|$ across the incident shock C_1 and the deflection ϑ_{02} across the separation shock C_2 (with respect to $\langle\vartheta_0\rangle = 0.2$). —— Time-averaged values. Maximum and minimum value detected in spanwise direction at each time instance are indicted by the grey region. $(d)-(e)$: Instantaneous snapshots at $t_1 = 2257$ and $t_2 = 2341$.

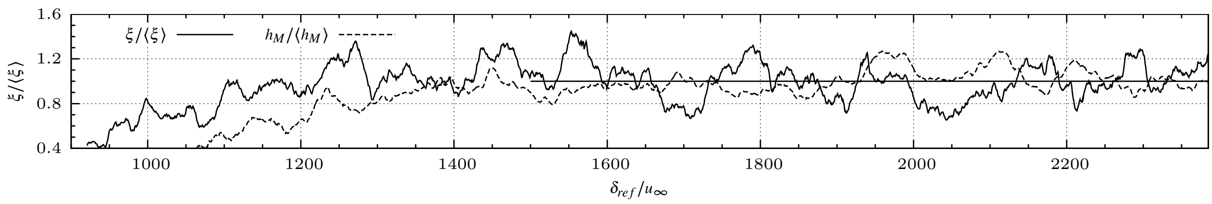

Figure 9: Evolution of the fluid mass per unit span ξ within the separation zone (——) and of the Mach stem height h_M (----), normalized by its time-averaged mean value.